Editors' Suggestion

Competing Fractional Quantum Hall and Electron Solid Phases in Graphene

Shaowen Chen,[1,2,*] Rebeca Ribeiro-Palau,[1,3,*,†] Kang Yang,[4,5] Kenji Watanabe,[6] Takashi Taniguchi,[6] James Hone,[3] Mark O. Goerbig,[4] and Cory R. Dean[1,‡]

[1]*Department of Physics, Columbia University, New York, 10027 New York, USA*
[2]*Department of Applied Physics and Applied Mathematics, Columbia University, New York, 10027 New York, USA*
[3]*Department of Mechanical Engineering, Columbia University, New York, 10027 New York, USA*
[4]*Laboratoire de Physique des Solides, CNRS UMR 8502, Université Paris-Sud, Université Paris Saclay, 91405 Orsay cedex, France*
[5]*LPTHE, CNRS-Université Pierre et Marie Curie, Sorbonne Universités, 4 Place Jussieu, 75252 Paris Cedex 05, France*
[6]*National Institute for Materials Science, 1-1 Namiki, 305-0044 Tsukuba, Japan*

(Received 30 July 2018; published 18 January 2019)

We report experimental observation of the reentrant integer quantum Hall effect in graphene, appearing in the $N = 2$ Landau level. Similar to high-mobility GaAs/AlGaAs heterostructures, the effect is due to a competition between incompressible fractional quantum Hall states, and electron solid phases. The tunability of graphene allows us to measure the B-T phase diagram of the electron solid phase. The hierarchy of reentrant states suggests spin and valley degrees of freedom play a role in determining the ground state energy. We find that the melting temperature scales with magnetic field, and construct a phase diagram of the electron liquid-solid transition.

DOI: 10.1103/PhysRevLett.122.026802

Electrons confined to two dimensions and subjected to strong magnetic fields can host a variety of fascinating correlated electron phases. One of the most widely studied examples is the fractional quantum Hall effect (FQHE) [1–4], an incompressible liquid that emerges when the lowest energy Landau levels (LLs) are partially filled. However, the incompressible FQHE liquids are not the only correlated phases that can emerge within partially filled LLs and generically compete with the formation of interaction-driven electron solids, such as the Wigner crystal [5–8], and the bubble [9–18] and stripe charge density wave states [9,11,12,16,17,19].

In GaAs/AlGaAs heterostructures, the competition between these different phases, particularly developed in the $N = 1$ and 2 LL, gives rise to a reentrant integer quantum Hall effect (RIQHE) [14,20–23]. This is characterized by the emergence of vanishing longitudinal resistance at fractional filling between the usual sequence of FQHE states, but with Hall conductivity restored to the closest integer value. Numerous experimental [10,14,24–26] and theoretical studies [11,12,27] favor a collective origin for the RIQHE where the emergent electron solid, formed by electrons in the last partially filled LL, is pinned by the underlying impurity potential and thus has the same insulating response as individually localized electrons in the integer quantum Hall effect. However, many of the experimentally reported details, such as the relative energy scales between different RIQHE states and apparent particle-hole asymmetry within a LL [14,25] remain poorly understood.

The universality of the integer and fractional QHE found in a wide variety of high mobility 2D electron systems suggests that the formation of the electron solid should be equally ubiquitous. However, observation of the RIQHE has so far remained conspicuously limited to GaAs heterostructures. In this Letter, we report experimental observation of a RIQHE in monolayer graphene, appearing near 0.33 partial filling of the $N = 2$ LL, together with weakly formed FQHE states at $1/5$ in this same LL. Our results are in excellent agreement with recent theoretical calculations that suggest that the solid phase is stabilized and dominates over the FQHE liquid in graphene at these filling fractions [28–30]. The wide tunability of the carrier density in graphene allows us to map the evolution in both magnetic field and temperature of four distinct RIQHE states appearing within the lower spin branch of the $N = 2$ LL. Comparing their melting temperatures reveals an unexpected hierarchy that is consistent with a residual spin and/or valley symmetry, indicating that the expanded degrees of freedom in graphene play a role. For a single RIQHE we use the melting transition to construct the first B-T phase diagram of the bubble phase at a fixed filling fraction.

Magnetoresistance measurements were performed in electrostatically defined Hall bars of monolayer graphene [31]. The heterostructures were prepared by a dry layer assembly technique with edge contacts [32], using graphite flakes as both top and bottom gates [Fig. 1(a)]. In brief (see Supplemental Material [33] for more detail) the bottom gate spans the full width of the graphene layer whereas the top gate is etched into the shape of a Hall bar. The bottom gate is biased such that the outer boundary of the device is maintained at the zero-density charge neutrality point:

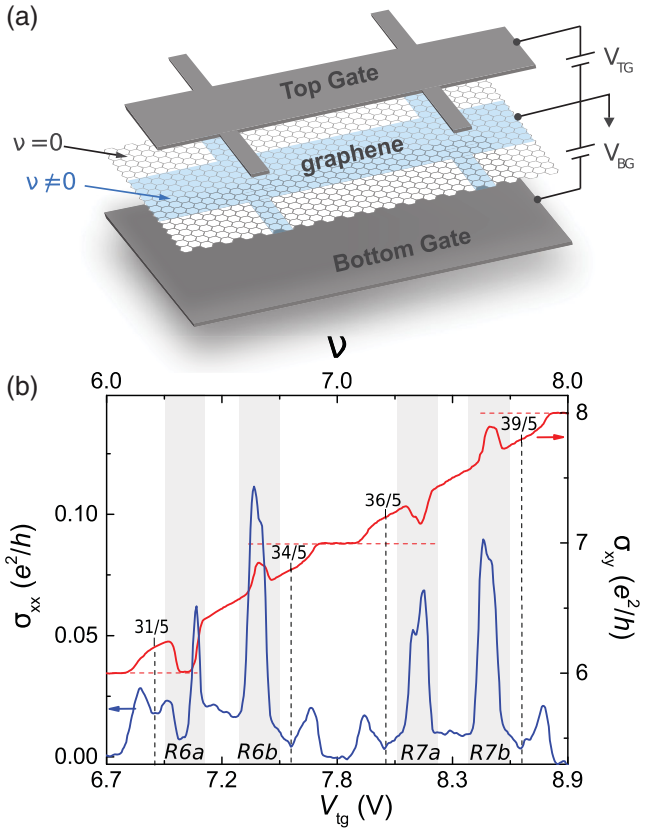

FIG. 1. RIQHE in the $N = 2$ LL of graphene. (a) Schematics of the gate defined Hall bar device used in this experiment. (b) Longitudinal (left axis) and Hall (right axis) conductivity as a function of the filling factor measured at $B = 23$ T and $T = 0.3$ K. Greyed regions highlight the four RIQHE and dashed vertical lines mark the four FQH states. Additionally, dashed horizontal lines mark the nearest integer value where the RIQHE is expected to be quantized.

because the $\nu = 0$ state in a graphene state is gapped at moderate fields both in the bulk and edge [38,39], this acts as a depletion region. The top graphite gate then acts as an accumulation gate, and is used to define the carrier density away from $\nu = 0$ in the Hall-bar shaped interior region of the device. Together this enables realization of a an electrostatically defined device [blue colored region in Fig. 1(a)].

Figure 1(b) shows the longitudinal (σ_{xx}) and Hall (σ_{xy}) conductivity for the lower spin branch of the $N = 2$ LL ($6 < \nu < 8$), measured at $B = 23$ T and $T = 0.3$ K. Four examples of the reentrant behavior can be identified, which we label $R6a$ and $R6b$ for the first valley branch and $R7a$ and $R7b$ for the other valley branch. We note that only the $R6a$ state is fully developed, with σ_{xy} showing a quantized plateau at $6e^2/h$, simultaneous with a well-developed minimum in σ_{xx}, where e is the electron charge and h is Planck's constant. For the remaining RIQHE states, where the Hall conductivity is not fully quantized, the longitudinal conductivity shows a large local maximum, consistent with previous observations in GaAs when the RIQHE states are not fully developed [14,20,21,24]. In addition to the RIQHE states, we observe signatures of weakly developed FQHE states at $\nu = 6 + 1/5$, $6 + 4/5$, $7 + 1/5$, and $7 + 4/5$ in the form of σ_{xx} minima simultaneous with kinks in the Hall conductivity (though not showing clear plateaus). Similar FQHE states have been previously reported in the third LL of ultrahigh mobility GaAs/AlGaAs samples [13]. Finally, we note that there is a clear absence of the $1/3$ FQHE states, which are the dominant FQHE states appearing in both $N = 0$ and $N = 1$ orbital branches of monolayer graphene [40,41]. Taken together these observations are in agreement with theoretical calculations indicating that charge density order is favored over a Laughlin FQHE state at $1/3$ filling in the $N = 2$ LL, but the FQHE is favored at $1/5$ filling {Fig. 2(a) as well as Ref. [29]}.

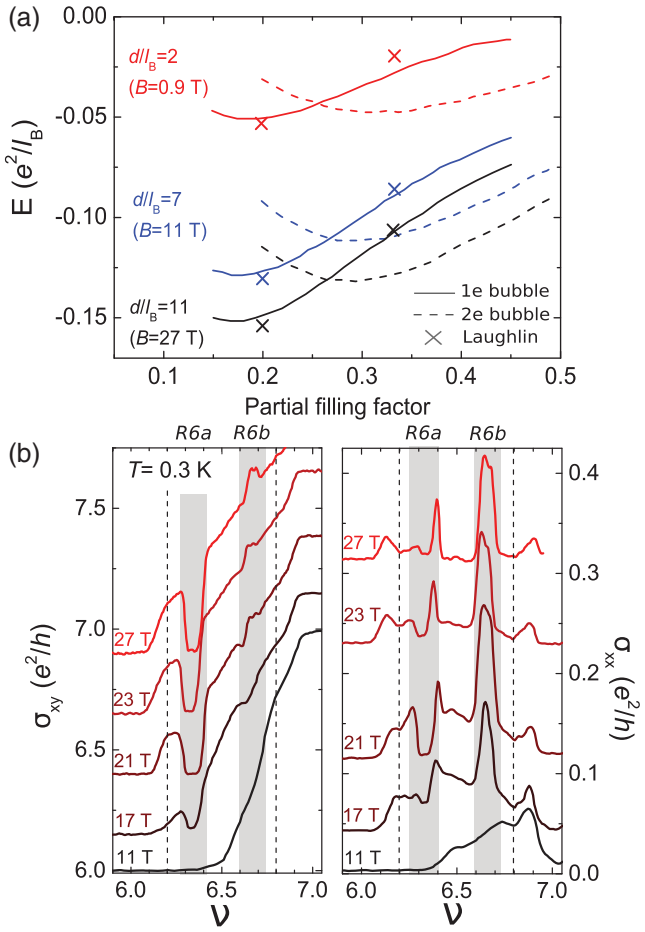

FIG. 2. Magnetic field dependence of the electron solid phase. (a) Numerical calculation of the energy as a function of filling for Laughlin and electron solid states in the $N = 2$ LL for different d/l_B ratio, where d is the distance to the metallic gates. The Laughlin states are represented by crosses while the one-electron and two-electron bubble phases are represented by solid and dashed lines, respectively. (b) Longitudinal (right) and Hall (left) conductivity as a function of filling factor for selected magnetic fields measured at 0.3 K. Dashed lines mark the presence of FQH states and greyed regions highlight the two RIQHE. Curves are vertically shifted for clarity.

Figure 2(a) shows the theoretically calculated energy of the electron solid and FQHE states for magnetic fields up to $B = 27$ T. The energies of the crystalline phases have been calculated within the Hartree-Fock approximation, while those of the liquid FQH states have been obtained with the help of the plasma sum rules [12,29]. In addition, we take into account explicitly the present experimental setup with metallic gates at a distance of 27 nm below and above the graphene sheet. They screen the effective Coulomb interaction as a function of d/l_B (see Supplemental Material [33] for further details), where d is the distance between the gates, $l_B = \sqrt{\hbar/eB}$ is the magnetic length.

At all magnetic fields considered we find that the electron solid is theoretically favorable over a FQHE at $1/3$ filling, but the situation remains reversed at $1/5$ filling with the FQHE state expected to be the ground state. In Fig. 2(b), we plot the evolution of the measured longitudinal and Hall conductivity in the filling factor range $\nu = 6$ to 7, for magnetic field ranging from 11 T to 27 T. At $B = 27$ T we observe a well developed $R6a$ but only weakly developed $R6b$ state, in addition to weakly formed FQHE states at $1/5$ and $4/5$ fillings, consistent with expectation. As we decrease the magnetic field, the $R6b$ state quickly disappears. By contrast the more robust $R6a$ varies in width but remains well quantized at least down to 17 T. The observed electron-hole asymmetry between the $R6a$ and $R6b$ is not anticipated by theoretical calculations, instead we expect these to be simple copies of each other [29,30,42,43].

At lower magnetic fields, $B = 11$ T, an unexpected behavior is observed near $R6a$, where the $\nu = 6$ integer QHE features, i.e., the Hall plateau and zero longitudinal conductivity, become extended and merge with $R6a$ features. This same behavior is not observed near the $\nu = 7$ plateau, where instead, at this same field, signatures of the $6 + 4/5$ FQHE state remain and the $R6b$ features have simply disappeared, giving way to an electron liquid. We interpret the extended $\nu = 6$ plateau to indicate that, in this field range, an electron solid state also exists near $1/5$ filling. This is not in agreement with the calculations shown in Fig. 2(a) and so the origin of this behavior is uncertain. We note that a similar transition of the electron solid as a function of magnetic field has been observed in the GaAs/AlGaAs quantum well system for the lowest LL when measured at different carrier densities [44]. In that study it was argued to be a quantum well width effect. However this is unlikely in our case since electrons are confined to a single atomic layer. We conjecture that, in the low field limit, an additional impurity potential may favor the electron solid phase over the FQHE near $1/5$ filling. Indeed, allowing for local deformations of the lattice, an electron solid can profit more efficiently from the impurity potential than the incompressible FQH states [12], theoretically inverting the relative ground state energies. The onset of this behavior in the low B limit could reflect a competition between the Coulomb and impurity energy scales. We note also that we generally observe the reentrant state to become better developed with successive cooldowns (see Supplemental Material [33]). Assuming that the disorder increases after a thermal cycle, this observation would be consistent with the disorder playing a role in stabilizing the RIQHE state.

Finally, we consider the temperature dependence of the RIQHE states. The critical temperature (T_c), where the electron solid undergoes a phase transition and melts into an electron liquid [14,25], provides a convenient estimate of the energy scale associated with the solid phase. Figure 3 shows the longitudinal resistance versus temperature for filling fractions $\nu = 6$ to 8, measured at $B = 23$ T. The four RIQHE states, $R6a$, $R6b$, $R7a$, and $R7b$, identified in this plot by a resistive peak (red) appear to melt at different critical temperatures. The qualitative trend in the apparent melting temperatures shows a relative hierarchy with $T_c^{R6a} > T_c^{R6b}$, while $T_c^{R7a} < T_c^{R7b}$. This difference in the a and b instances of the RIQHE suggest that the two states are not related by electron-hole symmetry within a single spin-valley branch. This result is unexpected [25], since spin and valley degrees of freedom are not anticipated to play a role and the two RIQHE states are instead expected to be merely two spin copies of the same state, with identical melting temperatures. We note that due to the elevated magnetic field (23 T) it is not possible for us to access the upper spin branch using the top gate. However, the hierarchy is suggestive, appearing symmetric at least across the entire spin branch. This symmetry reflects a

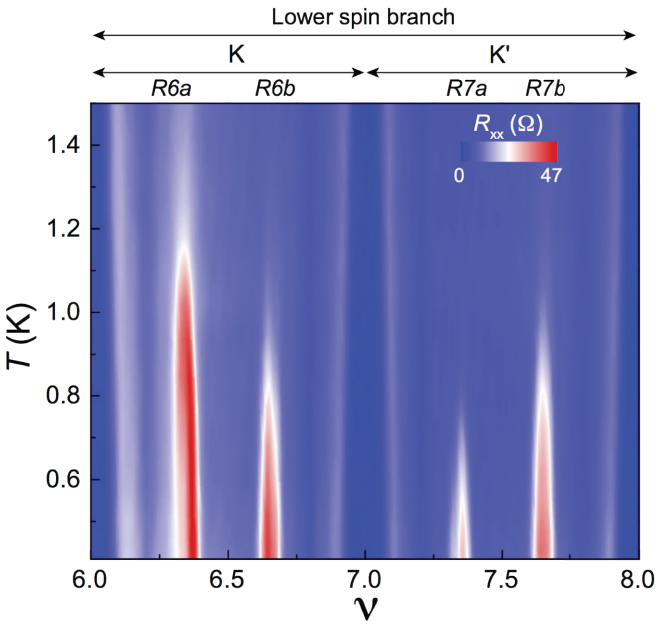

FIG. 3. Broken valley symmetry for the RIQHE of graphene. Longitudinal resistance as a function of filling factor and temperature, measured at 23 T, for the lower spin branch of the $N = 2$ LL.

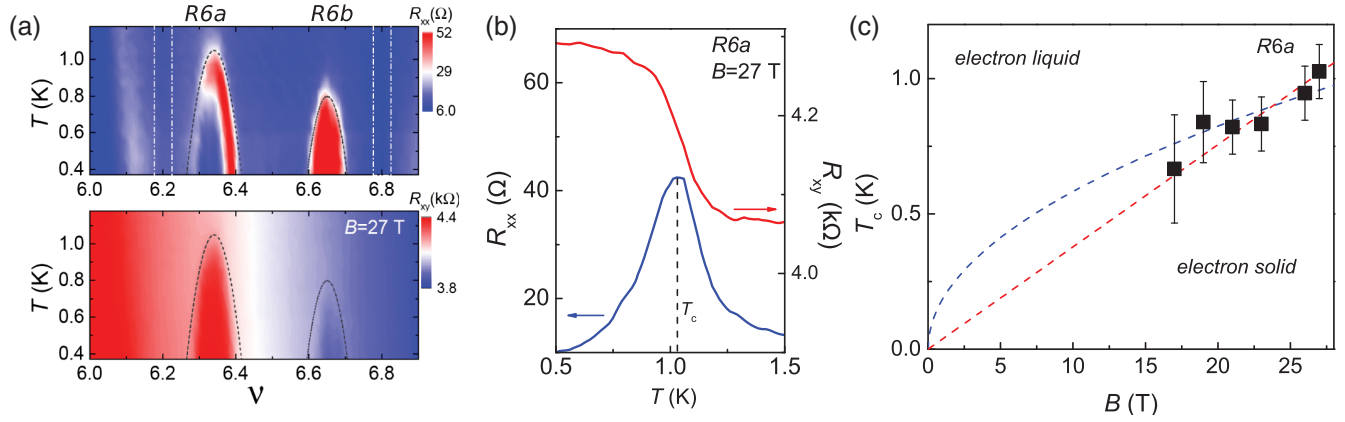

FIG. 4. Temperature dependence of the electron solid phase. (a) Longitudinal and Hall resistance as a function of filling factor and temperature for the *R6a* and *R6b* reentrant states, measured at 27 T. White dashed boxes mark the FQH state $\nu = 6 + 1/5$ and $\nu = 6 + 4/5$. Gray dashed lines indicate boundaries, using parabolic function $T_c(\bar{\nu}) = T_c(\bar{\nu_c}) - \beta(\bar{\nu} - \bar{\nu_c})^2$ for each RIQHE, consistent with [25]. (b) line cut at $\nu = 6.35$ for R_{xx} (left axis) and R_{xy} (right axis) at 27 T. (c) *B*-*T* phase diagram of the *R6a* state, dashed red line is the linear fit, dashed blue line is the square root fit.

similar hierarchy identified in the FQHE states of the $N = 1$ LL of monolayer graphene [45–47], where it has been suggested that spin and valley degeneracies are only partially lifted, and an approximate SU(2) or SU(4) symmetry is preserved for the composite Fermion ground states. Our observation of a similar hierarchy in the RIQHE of the $N = 2$ LL suggests that similarly these degeneracies may be only partially lifted, and, moreover, this order plays a role in the ground state energy of the solid phase as well.

Figures 4(a) and 4(b) show high resolution maps of the temperature evolution of longitudinal and Hall resistance for the *R6a* and *R6b*, acquired at $B = 27$ T. The *R6a* state is sufficiently well developed that we can quantitatively study its phase boundary. As the temperature is reduced, the resistance peak associated with *R6a* state splits, while the reentrant Hall plateau grows wider in ν. The filling fraction boundary of both features follows an approximate parabolic shape, similar to what has been reported in GaAs [25].

Figure 4(b) shows the temperature dependence of R_{xx} and R_{xy} acquired at $\nu = 6.35$, where the melting temperature is a maximum. As the temperature is lowered, R_{xx} increases to a maximum and then decreases, while R_{xy} increases from its classical Hall effect value to a quantized integer QHE level. Following Ref. [25], we take the temperature where R_{xx} is maximal to define the melting temperature T_c, of the solid phase. At 27 T, the *R6a* state has a T_c of about 1 K.

Extracting the melting temperature of *R6a* at different magnetic fields, we construct a *B*-*T* phase diagram, shown in Fig. 4(c). The melting temperature decreases as the magnetic field decreases. The electron solid state is driven by Coulomb interaction so a $\sqrt{B}$ dependence is expected [25]. On the other hand, a linear trend can also be expected due to screening from the top and back gates. This effect can be illustrated in the case of a single gate at a distance $d/2$ from the graphene layer, where the mirror charge creates a dipole and the interaction becomes dipolar at long distances (see Supplemental Material [33]). The energy scale $E_c = e^2/4\pi\epsilon l_B \propto \sqrt{B}$ (Coulomb) thus needs to be roughly replaced by $E_d = (e^2/4\pi\epsilon l_B) \times (d/l_B) \propto d \times B$ (dipolar). Naturally, one expects the effect to saturate in the large d/l_B limit, where the dipolar interaction is no longer justified. However, our measurement is made in an intermediate regime, where this expansion remains well justified. Over the field range where we can resolve the RIQHE, the linear and square root fit equally well and we are unable to discriminate these dependencies. Further study is needed to resolve these differences.

In conclusion, we have observed RIQHE in the $N = 2$ LL in graphene. The magnetic field evolution of states suggests a crossover of the energy competition between electron liquid and solid states. The temperature dependence of the states indicates a surprising hierarchy between the RIQHE states consistent with an approximate SU(2) or SU(4) symmetry being preserved. We have extracted the onset temperature and constructed the *B*-*T* phase diagram of the electron solid state. Our work opens the door of RIQHE study in a new, tunable material system, which contributes to the understanding of electron solid state in quantum Hall systems.

We thank G. Csáthy, J. I. A. Li, M. Yankowitz, and S. Dietrich for helpful discussions. S. Chen is supported by the ARO under MURI W911NF-17-1-0323. This research was supported by the NSF MRSEC program through Columbia in the Center for Precision Assembly of Superstratic and Superatomic Solids (DMR-1420634). A portion of this work was performed at the National High Magnetic Field Laboratory, which is supported by National Science Foundation Cooperative Agreement No. DMR-1157490 and the State of Florida.

*S. Ch. and R. R.-P. contributed equally to this work.
†Present address: Centre de Nanosciences et de Nanotechnologies (C2N), CNRS, Univ Paris Sud, Université Paris-Saclay, 91120 Palaiseau, France.
rebeca.ribeiro@c2n.upsaclay.fr
‡cd2478@columbia.edu

[1] D. C. Tsui, H. L. Stormer, and A. C. Gossard, Phys. Rev. Lett. **48**, 1559 (1982).
[2] R. B. Laughlin, Phys. Rev. Lett. **50**, 1395 (1983).
[3] F. D. M. Haldane, Phys. Rev. Lett. **51**, 605 (1983).
[4] J. K. Jain, Phys. Rev. Lett. **63**, 199 (1989).
[5] E. Wigner, Phys. Rev. **46**, 1002 (1934).
[6] Yu. P. Monarkha and V. E. Syvokon, Low Temp. Phys. **38**, 1067 (2012).
[7] I. L. Drichko, I. Y. Smirnov, A. V. Suslov, Y. M. Galperin, L. N. Pfeiffer, and K. W. West, Phys. Rev. B **94**, 075420 (2016).
[8] I. L. Drichko, I. Y. Smirnov, A. V. Suslov, L. N. Pfeiffer, K. W. West, and Y. M. Galperin, Phys. Rev. B **92**, 205313 (2015).
[9] M. M. Fogler, A. A. Koulakov, and B. I. Shklovskii, Phys. Rev. B **54**, 1853 (1996).
[10] R. M. Lewis, P. D. Ye, L. W. Engel, D. C. Tsui, L. N. Pfeiffer, and K. W. West, Phys. Rev. Lett. **89**, 136804 (2002).
[11] M. O. Goerbig, P. Lederer, and C. Morais Smith, Phys. Rev. B **68**, 241302 (2003).
[12] M. O. Goerbig, P. Lederer, and C. M. Smith, Phys. Rev. B **69**, 115327 (2004).
[13] G. Gervais, L. W. Engel, H. L. Stormer, D. C. Tsui, K. W. Baldwin, K. W. West, and L. N. Pfeiffer, Phys. Rev. Lett. **93**, 266804 (2004).
[14] N. Deng, J. D. Watson, L. P. Rokhinson, M. J. Manfra, and G. A. Csáthy, Phys. Rev. B **86**, 201301 (2012).
[15] W. Pan, A. Serafin, J. S. Xia, L. Yin, N. S. Sullivan, K. W. Baldwin, K. W. West, L. N. Pfeiffer, and D. C. Tsui, Phys. Rev. B **89**, 241302 (2014).
[16] R. R. Du, D. C. Tsui, H. L. Stormer, L. N. Pfeiffer, K. W. Baldwin, and K. W. West, Solid State Commun. **109**, 389 (1999).
[17] M. Lilly, K. Cooper, J. Eisenstein, L. Pfeiffer, and K. West, Phys. Rev. Lett. **82**, 394 (1999).
[18] V. Shingla, E. Kleinbaum, A. Kumar, L. N. Pfeiffer, K. W. West, and G. A. Csáthy, Phys. Rev. B **97**, 241105 (2018).
[19] R. Moessner and J. T. Chalker, Phys. Rev. B **54**, 5006 (1996).
[20] J. P. Eisenstein, K. B. Cooper, L. N. Pfeiffer, and K. W. West, Phys. Rev. Lett. **88**, 076801 (2002).
[21] J. S. Xia, W. Pan, C. L. Vicente, E. D. Adams, N. S. Sullivan, H. L. Stormer, D. C. Tsui, L. N. Pfeiffer, K. W. Baldwin, and K. W. West, Phys. Rev. Lett. **93**, 176809 (2004).
[22] A. Kumar, G. A. Csáthy, M. J. Manfra, L. N. Pfeiffer, and K. W. West, Phys. Rev. Lett. **105**, 246808 (2010).
[23] W. Li, D. R. Luhman, D. C. Tsui, L. N. Pfeiffer, and K. W. West, Phys. Rev. Lett. **105**, 076803 (2010).
[24] R. Lewis, Y. P. Chen, L. Engel, D. Tsui, L. Pfeiffer, and K. West, Phys. Rev. B **71**, 081301 (2005).
[25] N. Deng, A. Kumar, M. J. Manfra, L. N. Pfeiffer, K. W. West, and G. A. Csáthy, Phys. Rev. Lett. **108**, 086803 (2012).
[26] X. Wang, H. Fu, L. Du, X. Liu, P. Wang, L. N. Pfeiffer, K. W. West, R.-R. Du, and X. Lin, Phys. Rev. B **91**, 115301 (2015).
[27] M. O. Goerbig, P. Lederer, and C. Morais Smith, Phys. Rev. Lett. **93**, 216802 (2004).
[28] Z. Papić, D. A. Abanin, Y. Barlas, and R. N. Bhatt, Phys. Rev. B **84**, 241306 (2011).
[29] M. E. Knoester, Z. Papić, and C. Morais Smith, Phys. Rev. B **93**, 155141 (2016).
[30] C.-H. Zhang and Y. N. Joglekar, Phys. Rev. B **75**, 245414 (2007).
[31] R. Ribeiro-Palau, S. Chen, Y. Zeng, K. Watanabe, T. Taniguchi, J. Hone, and C. Dean, arXiv:1901.01277.
[32] L. Wang, I. Meric, P. Y. Huang, Q. Gao, Y. Gao, H. Tran, T. Taniguchi, K. Watanabe, L. M. Campos, D. A. Muller, J. Guo, P. Kim, J. Hone, K. L. Shepard, and C. R. Dean, Science **342**, 614 (2013).
[33] See Supplemental Material at http://link.aps.org/supplemental/10.1103/PhysRevLett.122.026802 for further details on device characterization, experimental results and theoretical description, which includes Ref. [34–37].
[34] D. Levesque, J. J. Weis, and A. H. MacDonald, Phys. Rev. B **30**, 1056 (1984).
[35] S. M. Girvin, A. H. MacDonald, and P. M. Platzman, Phys. Rev. B **33**, 2481 (1986).
[36] M. M. Fogler and A. A. Koulakov, Phys. Rev. B **55**, 9326 (1997).
[37] R. M. Lewis, Y. Chen, L. W. Engel, D. C. Tsui, P. D. Ye, L. N. Pfeiffer, and K. W. West, Phys. Rev. Lett. **93**, 176808 (2004).
[38] A. F. Young, C. R. Dean, L. Wang, H. Ren, P. Cadden-Zimansky, K. Watanabe, T. Taniguchi, J. Hone, K. L. Shepard, and P. Kim, Nat. Phys. **8**, 550 (2012).
[39] A. Young, J. Sanchez-Yamagishi, B. Hunt, S. Choi, K. Watanabe, T. Taniguchi, R. Ashoori, and P. Jarillo-Herrero, Nature (London) **505**, 528 (2014).
[40] C. R. Dean, A. F. Young, P. Cadden-Zimansky, L. Wang, H. Ren, K. Watanabe, T. Taniguchi, P. Kim, J. Hone, and K. L. Shepard, Nat. Phys. **7**, 693 (2011).
[41] F. Amet, A. Bestwick, J. Williams, L. Balicas, K. Watanabe, T. Taniguchi, and D. Goldhaber-Gordon, Nat. Commun. **6**, 5838 (2015).
[42] O. Poplavskyy, M. O. Goerbig, and C. Morais Smith, Phys. Rev. B **80**, 195414 (2009).
[43] M. O. Goerbig, Rev. Mod. Phys. **83**, 1193 (2011).
[44] Y. Liu, C. G. Pappas, M. Shayegan, L. N. Pfeiffer, K. W. West, and K. W. Baldwin, Phys. Rev. Lett. **109**, 036801 (2012).
[45] B. E. Feldman, B. Krauss, J. H. Smet, and A. Yacoby, Science **337**, 1196 (2012).
[46] Y. Zeng, J. Li, S. Dietrich, O. Ghosh, K. Watanabe, T. Taniguchi, J. Hone, and C. Dean, arXiv:1805.04904.
[47] H. Polshyn, H. Zhou, E. Spanton, T. Taniguchi, K. Watanabe, A. F. Young *et al.*, Phys. Rev. Lett. **121**, 226801 (2018).